Mon. Not. R. Astron. Soc. **000**, 000–000 (0000) Printed 17 January 2013 (MN LaTeX style file v2.2)

arXiv:1301.3673v1 [astro-ph.CO] 16 Jan 2013

BAOs and Non-linearities: 3D Spherical Analysis

Geraint Pratten and Dipak Munshi
School of Physics and Astronomy, Cardiff University, Queen's Buildings, 5 The Parade, Cardiff, CF24 3AA, UK

17 January 2013, Revision: 0.9

ABSTRACT

The Baryon Acoustic Oscillations (BAO) are features in the matter power spectrum on scales of order 100 - 150 h^{-1}Mpc that promise to be a powerful tool to constrain and test cosmological models. The BAO have attracted such attention that future upcoming surveys have been designed with the BAO at the forefront of the primary science goals. Recent studies have advocated the use of a spherical-Fourier Bessel (SFB) expansion for future wide field surveys that cover both wide and deep regions of the sky necessitating the simultaneous treatment of the spherical sky geometry as well as the extended radial coverage. In this paper we present and extended analysis of the BAO's using the SFB formalism by taking into account the role of non-linearities in the oscillations observed in the galaxy power spectrum. The SFB power spectrum has both radial and tangential dependence and it has been shown that in the limit that we approach a deep survey the SFB power spectrum is purely radial and collapses to the Cartesian Fourier power spectrum. This radialisation of information is shown to hold even in the presence of redshift space distortions and 1-loop corrections to the galaxy power spectrum albeit with modified tangential and radial dependence. As per previous studies we find that the introduction of non-linearities leads to a damping of the oscillations in the matter power spectrum.

Key words: : Cosmology– Cosmic Microwave Background Radiation- Large-Scale Structure of Universe – Methods: analytical, statistical, numerical

1 INTRODUCTION

Observations of the cosmic microwave background (CMB) and large-scale structure (LSS) will carry complementary cosmological information. While all-sky CMB observations, such as NASA'a WMAP or ESA'a Planck experiments, primarily probe the distribution of matter and radiation at redshift $z = 1300$, large scale surveys such as ESA's Euclid or the SKA will provide a window at lower redshifts on order $z \approx 0 - 2$. The study of large scale structure appears to be a promising candidate in the study of the influence and role of the dark sectors in the standard model of cosmology. One particular phenomena of interest are the Baryon Acoustic Oscillations (BAOs) that manifest themselves in the matter power spectrum of galaxy clusters on cosmological scales of order $100h^{-1}Mpc$. These oscillations in the matter power spectrum are generated just before recombination through the interplay between a coupled photon-baryon fluid and gravitationally interacting dark matter (Sunyaev and Zeldovich 1970; Peebles and Yu 1970; Eisenstein et al 2005; Seo and Eisenstein 2003, 2007).

The scale of the peaks and oscillatory features of the BAOs promises to be an important cosmological tool that acts as a standard ruler from which we can investigate and constrain dark energy parameters (see Eisenstein et al (2005); Amendola, Quercellini and Giallongo (2005); Dolney, Jain and Takada (2006); Wang and Mukherjee (2006) for a small selection or representative literature), neutrino masses (Goobar, Hannestad, Mrtsell and Tu 2006), modified theories of gravitation (Alam and Sahni 2006; Lazkoz, Maartens and Majerotto 2006) and deviations from the standard model of cosmology (Garcia-Bellido and Haugboelle 2008, 2009; February, Clarkson and Maartens 2012)). Significant attention has been devoted to the BAOs and they were first detected with SDSS data (Eisenstein et al 2005; Adelman-McCarthy et al 2008) and in subsequent surveys (Colless et al 2003; Percival et al 2007).

The BAOs have been studied using standard Fourier space decompositions (Seo and Eisenstein 2003, 2007), real space analysis (Eisenstein et al 2005; Slosar, Ho, White and Louis 2009; Xu et al 2010; Juszkiewicz, Hellwing and van de Weygaert 2012), in 2D

© 0000 RAS

spherical harmonics defined on thin spherical shells (Dolney, Jain and Takada 2006), but also in a spherical Fourier-Bessel expansion (Rassat and Refregier 2012). It is important to note that different frameworks will make use of different information and will therefore have different constraining power for different cosmological parameters emphasising the complementarity of mixed studies (Rassat et al 2008). Previous studies, having predominantly focused on projected 2D surveys, have discarded statistical information by projecting galaxy positions into tomographic redshift bins however, such a loss of information could be avoided by adopting a full 3D description (Asorey et al 2012).

Upcoming large scale structure surveys will provide cover for both large and deep areas of the sky and this will necessitate a formalism that can provide a simultaneous treatment of both the spherical sky geometry as well as an extended radial coverage. A natural basis for such a survey is provided by the spherical Fourier-Bessel (SFB) decomposition, see (Heavens and Taylor 1995; Fisher et al 1995; Percival et al 2004; Castro, Heavens and Kitching 2005; Erdogdu et al 2006; Abramo, Reimberg and Xavier 2010; Leistedt et al 2011; Shapiro, Crittenden and Percival 2011; Rassat and Refregier 2012; Lanusse, Rassat and Starck 2012; Asorey et al 2012) for an incomplete selection of literature on the subject. In this prescription we expand a 3D tracer field, such as the galaxy density contrast, using the radial (k) and tangential (i.e. along the surface of a sphere) (l) dependence.

The galaxy matter power spectrum, as an initial approach, is often modelled using cosmological perturbation theory (PT) at linear order. However, linear PT will break down due to the nonlinear growth of structure under gravitational instability. This necessitates the use of non-linear (or higher order) PT. In addition real world observations are plagued by the presence of nonlinear contributions to the power spectrum. The main sources of non-linearity that we must take into account include:

- Non-linear evolution of matter density field and it's perturbations. This will give rise to correction to the linear matter power spectrum.
- Non-linear galaxy clustering bias arising from a non-linear mapping between the underlying matter density field and observed collapsed objects (e.g. galaxies or DM Haloes). Galaxy clustering bias also modifies the matter power spectrum.
- Redshift space distortions arising from the peculiar velocities of galaxies manifest themselves in the observed redshifts of galaxy surveys. RSD give rise to systematic effects in the redshift space matter power spectrum that differ from the real space matter power spectrum.
- Non-Gaussian corrections to the initial density field. In this paper we assume Gaussian initial conditions.

In this paper we will follow the construction outlined in Rassat and Refregier (2012) and generalise the method to study the role of redshift space distortions (RSD) and the non-linear (NL) evolution of density perturbations. Previous investigations have used standard perturbation theory (SPT), galaxy bias models and Lagrangian perturbation theory to characterise the role of various non-linear corrections to the BAO signal using the 3D Fourier power spectrum $P(k)$ (Jeong and Komatsu 2006; Nishimichi et al 2007; Jeong and Komatsu 2009; Nomura, Yamamoto and Nishimichi 2008; Nomura, Yamamoto, Huetsi and Nishimichi 2009). These nonlinear corrections can be reassessed within the SFB framework to aid our understanding of how real world effects can impact the radialisation of information.

Recent work (Asorey et al 2012) utilising the SFB formalism has focused on how to recover the full 3D clustering information including RSD from 2D tomography using the angular auto and cross spectra of different redshift bins. Traditionally, RSD measurements have been made through spectroscopic redshift surveys such as the 2dF Galaxy Redshift Survey (Colless et al 2003) and the Sloan Digital Sky Survey (York et al 2000) with photometric surveys often being neglected because of the loss of RSD through photometric redshift errors. Upcoming surveys, spectroscopic and photometric, such as the Dark Energy Survey (DES www.darkenergysurvey.org), Euclid (sci.esa.int/euclid), Square Kilometer Array (SKA www.skatelescope.org), Physics of the Accelerating Universe Survey (PAU www.pausurvey.org) (Bentez et al 2009), Large Synoptic Survey Telescope (LSST www.lsst.org) or the Panoramic Survey Telescope and Rapid Response System (PanStarrs pan-starrs.ifa.hawaii.edu) offer the possibility of investigating the BAO and RSD through angular or projected clustering measurements Bentez et al (2009); Nock, Percival and Ross (2010); Crocce, Fosalba, Castander and Gaztanaga (2010); Gaztanaga et al (2011); Laureijs et al (2011); Ross, Percival, Crocce, Cabr and Gaztanaga (2011).

As RSD and distortions arising from an incorrect assumption for the underlying geometry are similar (Alcock and Paczynski 1979) the analyses of RSD using 3D data has to be used in conjunction with geometrical constraints. Approaches based purely on angular correlation functions, depending only on the redshift and angles, do not depend on the background cosmological model making angular clustering measures considerably simpler in this respect. The SFB is something of a mid-point between these two extremes and will, in general, be sensitive to the choice of fiducial concordance cosmology.

This paper is organised as follows. In §2 we discuss the Spherical Fourier-Bessel (SFB) Expansion in the context of redshift-space distortions. In §3 we add the perturbative corrections to linear power-spectrum. Results are discussed in §4 and finally the conclusions are presented in §5. Discussions about finite size of the survey and discrete Spherical Fourier-Bessel (SFB) transforms are relegated to an appendix.

Throughout we will adopt the WMAP 7 cosmological parameters (Komatsu et al 2011): $h = 0.7, \Omega_b h^2 = 0.0226, \Omega_c h^2 = 0.112, \Omega_\Lambda = 0.725, \sigma_8 = 0.816$.

2 REDSHIFT SPACE DISTORTIONS

2.1 Spherical Fourier-Bessel (SFB) Expansion

Spherical coordinates are a natural choice for the analysis of cosmological data as they can, by an appropriate choice of basis, be used to place an observer at the origin of the analysis. Upcoming wide-field BAO surveys will provide both large and deep coverage of the sky and we therefore require a simultaneous treatment of the extended radial coverage and spherical sky geometry. For this problem, the spherical Fourier-Bessel expansion is a natural basis for the analysis of random fields in such a survey.

We introduce a homogeneous 3D random field $\Psi(\hat{\Omega}, r)$ where $\hat{\Omega}$ defines the position on the surface of a sphere and r denotes the comoving radial distance. The eigenfunctions of the Laplacian operators are constructed from products of the spherical Bessel functions of the first kind $j_l(kr)$ and spherical harmonics $Y_{lm}(\hat{\Omega})$ with eigenvalues of $-k^2$ for a 2-sphere. Assuming a flat geometry, the random field can be harmonically decomposed into the spherical Fourier-Bessel basis, which is both complete and orthonormal, with the expansion given by:

$$\Psi(\hat{\Omega}, r) = \sqrt{\frac{2}{\pi}} \int dk \sum_{\{lm\}} \Psi_{lm}(k)\, k\, j_l(kr) Y_{lm}(\hat{\Omega}), \qquad (1)$$

and the corresponding inverse relation given by:

$$\Psi_{lm}(k) = \sqrt{\frac{2}{\pi}} \int d^3\mathbf{r}\, \Psi(\mathbf{r})\, k\, j_l(kr) Y^*_{lm}(\hat{\Omega}). \qquad (2)$$

In our notation $\{lm\}$ are quantum numbers and k is the wavenumber. Note that the 3D harmonic coefficients, $\Psi_{lm}(k)$ are a function of the radial wavenumber k. This decomposition can be viewed as the spherical polar analogy to the conventional Cartesian Fourier decomposition defined by:

$$\Psi(\mathbf{r}) = \frac{1}{(2\pi)^{3/2}} \int d^3k\, \Psi(k)\, \mathrm{e}^{\mathbf{ik\cdot r}}, \qquad (3)$$

$$\Psi(\mathbf{k}) = \frac{1}{(2\pi)^{3/2}} \int d^3x\, \Psi(\mathbf{r})\, \mathrm{e}^{-\mathbf{ik\cdot r}}. \qquad (4)$$

The Fourier power spectrum, $P_{\Psi\Psi}$, is defined as the 2-point correlation function of the Fourier coefficients $\Psi(k)$,

$$\langle \Psi(\mathbf{k})\Psi^*(\mathbf{k}')\rangle = (2\pi)^3 P_{\Psi\Psi}(k)\delta^3\left(\mathbf{k} - \mathbf{k}'\right). \qquad (5)$$

Similarly we can define a 3D SFB power spectrum, $C_l(k)$, of our random field by calculating the 2-point correlation function of the 3D harmonic coefficients,

$$\langle \Psi_{lm}(k)\Psi^*_{l'm'}(k')\rangle = \mathcal{C}_l(k)\delta^{1\mathrm{D}}(k - k')\delta^{\mathrm{K}}_{ll'}\delta^{\mathrm{K}}_{mm'}. \qquad (6)$$

It is possible to relate the Fourier coefficients $\Psi(\mathbf{k})$ with their SFB analog $\Psi_{lm}(k)$ through the following expression,

$$\Psi_{lm}(k) = \frac{i^l}{(2\pi)^{3/2}} \int d\Omega_k \Psi(\mathbf{k}) Y_{lm}(\hat{\Omega}_k) \qquad (7)$$

where the angular position of the wave vector $\mathbf{k}$ in Fourier space is denoted by the unit vector $\hat{\Omega}(\theta_l, \phi_k)$. The Rayleigh-expansion of a plane wave is particularly useful in connecting the spherical harmonic description with the 3D Cartesian expression. The second expression we present here is derived by differentiating the first and will be used in the derivation of redshift space distortions:

$$\mathrm{e}^{\mathbf{ik\cdot r}} = 4\pi \sum_{\mathrm{lm}} \mathrm{i}^{\mathrm{l}}\, \mathrm{j_l(kr) Y_{lm}(\hat{\Omega}_k) Y_{lm}(\hat{\Omega})}; \qquad (8)$$

$$i(\hat{\Omega}_k \cdot \hat{\Omega})\mathrm{e}^{\mathbf{ik\cdot r}} = 4\pi \sum_{\mathrm{lm}} \mathrm{i}^{\mathrm{l}}\, \mathrm{j'_l(kr) Y_{lm}(\hat{\Omega}_k) Y_{lm}(\hat{\Omega})}. \qquad (9)$$

In general the radial eigenfunctions are ultra-spherical Bessel functions but they can be approximated by spherical Bessel functions when the curvature, of the Universe, is small. Throughout this paper we will use $j_l'(x)$ and $j_l''(x)$ to denote the first and second derivatives of $j_l(x)$ with respect to its argument x. The expressions for the first and second derivatives are given in Eq.(B2) and Eq.(B3). Imposing a finite boundary condition on the radial direction will result in a discreet sampling of the k-modes. This will be discussed in more detail later.

2.2 Selection Functions and Window Functions

In order to consider realistic cosmological random fields, such as the galaxy density contrast, we need to take into account the partial observation effects arising from finite survey volumes. This discussion will follow that of Rassat and Refregier (2012), including the discussion of the radial and tangential limits of the selection function. The selection function denotes the probability of including a galaxy within the survey.

An observed random field $\Psi^{obs}(\mathbf{r})$ can be related to our underlying 3D random field by a survey-dependent radial selection function $\phi(r)$,

$$\Psi^{obs}(\mathbf{r}) = \phi(r)\Psi(\mathbf{r}). \qquad (10)$$

It is possible to introduce and analogous tangential selection function but we will, as per Rassat and Refregier (2012), neglect this possibility assuming that we have data for the full sky. The selection function is typically normalised by the characteristic survey volume, V, defined such that as we take the volume to infinity we recover the underlying random field,

$$\lim_{V\to\infty} \Psi^{obs}(\mathbf{r}) = \Psi(\mathbf{r}). \qquad (11)$$

As homogeneity is broken, due to the introduction of the selection function, the SFB power spectrum now depends on k, k' and l and is given by:

$$\langle \Psi^{obs}_{lm}(k)\Psi^{obs*}_{l'm'}\rangle = \mathcal{C}^{obs}_l(k, k')\delta_{ll'}\delta_{mm'}, \qquad (12)$$

but can be shown to be expressed as follows (e.g. Rassat and Refregier (2012)):

$$\mathcal{C}^{00}_l(k_1, k_2) = \left(\frac{2}{\pi}\right)^2 \int k'^2 dk'\, I^0_l(k_1, k')I^0_l(k_2, k')P_{\delta\delta}(k') \qquad (13)$$

where the window function is defined as:

$$I^{(0)}_l(k, k') = \int dr\, r^2\phi(r)\, k\, j_l(kr)\, j_l(k'r). \qquad (14)$$

The SFB power spectrum tends to rapidly decay as we move away from the diagonal $k = k'$ and it will often be much more useful to focus purely on the diagonal contribution.

2.2.1 *Gaussian Selection Function*

A commonly adopted selection function is the Gaussian function,

$$\phi(r) = \mathrm{e}^{-(\mathrm{r/r_0})^2}, \qquad (15)$$

such that r_0 is a radius parameter defined by the normalisation of the survey volume, $V = \pi^{2/3} r_0^3$. It can be shown (Rassat and Refregier 2012) that the window function may be integrated analytically and reduces to:

$$I_l^{(0)}(k,k') = \frac{\pi r_0^2}{4}\sqrt{\frac{k}{k'}}\exp\left[-r_0^2\frac{k^2+k'^2}{4}\right] I_{l+\frac{1}{2}}\left(\frac{r_0^2 kk'}{2}\right). \tag{16}$$

2.2.2 *Radial Limit*

The radial limit corresponds to full radial coverage such that,

$$\phi(r) \to 1 \;\forall r \tag{17}$$

and the Gaussian window function is significantly simplified to

$$I_l(k,k') = \frac{\pi}{2k'}\delta\left(k-k'\right). \tag{18}$$

Using this asymptotic window function the power spectrum reduces to the Cartesian Fourier power spectrum (Rassat and Refregier 2012):

$$C_l^{\rm Obs}(k,k') = C_l(k)\delta(k-k') = P(k)\delta(k-k'). \tag{19}$$

2.2.3 *Tangential Limit*

The second case is defined in the limit that the selection function probes only a thin shell of the field at a distance r_* (Rassat and Refregier 2012),

$$\phi(r) = r_*\delta\left(r-r_*\right), \tag{20}$$

normalised such that $V = 4\pi r_*^3$. The corresponding convolution kernel, neglecting redshift space distortions, reduces to,

$$I_l^{(0)}(k,k') = r_*^3 j_l(kr_*) j_l(k'r_*) \tag{21}$$

2.3 Power Spectrum Evolution and Bias

The linear matter power spectrum at an arbitrary redshift z can be calculated by evolving the power spectrum according to

$$P_{\delta\delta}(k,z) = D^2(z)P_{\rm ini}(k)T^2(k) \tag{22}$$

where $T(k)$ is the conventional transfer function. The linear growth factor $D(z)$ is normalised to unity at present times and allows us to quantify the change in the linear growth of matter with respect to redshift. In a realistic galaxy survey, observations of galaxy density field contrast δ_g act as a tracer of the underlying matter distribution δ_m:

$$\delta_g = b(z,k)\delta_m \tag{23}$$

such that $b(k,z)$ is the galaxy bias. In general, the bias may be both redshift and scale dependent but we do not investigate the role of bias to any significant detail in this paper instead adopting a common adhoc functional form for the bias, $b(z) = \sqrt{1+z}$. Throughout we will assume that the bias is scale independence and therefore only modulates the overall amplitude of the galaxy power spectrum $P_g(k)$

$$P_g(k,z) = b^2(z)D^2(z)P_{\rm ini}(k)T^2(k). \tag{24}$$

2.4 Redshift Space Distortions

The measured distribution of galaxies is not without limits though as various systematic and survey dependent errors become more important. In practice, the observed galaxy redshift distributions are distorted due to the peculiar velocity of each galaxy. The anisotropy generated by the peculiar velocities is known as *redshift space distortion*. Although this distortion of the measured redshifts will necessarily complicate the cosmological interpretation of the spectroscopic galaxy surveys, the redshift space distortions are currently one of the most optimistic probes for the measurement of the growth rate of structure formation and, as a result, an interesting probe of models for dark energy and modified theories of gravity.

The effect of the redshift space distortions on the matter power spectrum can be split into two effects, the Kaiser effect and the Finger-of-God effect. The Kaiser effect corresponds to the coherent distortion of the peculiar velocity along the line of sight with an amplitude controlled by the growth-rate parameter. The Finger-of-God effect arises due to the random distribution of peculiar velocities leading to an incoherent contribution in which dephasing occurs and the clustering amplitude is suppressed. It is thought that the suppression of the amplitude is particularly important around the size of halo forming regions.

For an isotropic structure in linear theory, the Kaiser effect means that an observer will measure more power in the radial direction than in the transverse modes. The amplitude of this distortion is modulated by the distortion parameter

$$\beta = \frac{f(\Omega_0)}{b(z)} = \frac{1}{b(z)}\frac{d\ln D(a)}{d\ln a} \approx \frac{\Omega_M^{0.6}}{b(z)} \tag{25}$$

meaning that the RSD can be used as a probe of the growth of structure and of the galaxy clustering bias function $b(z)$.

The effect a peculiar velocity, or a departure from the Hubble flow, $v(\mathbf{r})$ at $\mathbf{r}$ is to introduce a distortion to the galaxy positions in the redshift space $\mathbf{s}$:

$$\mathbf{s}(\mathbf{r}) = \mathbf{r} + \mathbf{v}(\mathbf{r})\cdot\hat{\Omega}. \tag{26}$$

We denote the harmonics of a field $\Psi(\mathbf{r})$ when convolved with a selection function, $\phi(s)$, by $\tilde{\Psi}_{lm}(k)$. These harmonics take into account the redshift space distortions:

$$\tilde{\Psi}_{lm}(k) = \sqrt{\frac{2}{\pi}}\int s^2 ds \int d\hat{\Omega}\,\phi(s)\Psi(\mathbf{r})\,j_l(ks)Y_{lm}^*(\hat{\Omega}). \tag{27}$$

The Fourier transform of the linearised Euler equation can be used to relate the Fourier transform of the density contrast, $\delta(\mathbf{k})$, to that of the peculiar velocity field $v(\mathbf{r})$:

$$\mathbf{v}(\mathbf{k}) = -i\beta\mathbf{k}\frac{\delta(\mathbf{k})}{k^2} \tag{28}$$

where b is the linear bias parameter. Following the procedure outline in Heavens and Taylor (1995), we can establish a series expansion in β such that the lowest order coefficients $\Psi^{(0)}_{lm}(k)$ are obtained by neglecting the redshift space distortions:

$$\tilde{\Psi}_{lm}(k) = \tilde{\Psi}^{(0)}_{lm}(k) + \tilde{\Psi}^{(1)}_{lm}(k) + \ldots; \tag{29}$$

$$\tilde{\Psi}^{(0)}_{lm}(k) = \sqrt{\frac{2}{\pi}} \int_0^\infty k' dk' \; \Psi_{lm}(k') I^{(0)}_l(k', k); \tag{30}$$

$$\tilde{\Psi}^{(1)}_{lm}(k) = \sqrt{\frac{2}{\pi}} \int_0^\infty k' dk' \; \Psi_{lm}(k') I^{(1)}_l(k', k). \tag{31}$$

The kernels $I^{(0)}_l(k', k)$ and $I^{(0)}_l(k', k)$ define the convolution and are dependent on the choice of selection function. Note that $I^{(0)}_l(k', k)$ is simply the window function we encountered previously in Eq.(14). The kernels can be shown to be:

$$I^{(0)}_l(k, k') = \int dr\, r^2 \phi(r)\, k\, j_l(kr)\, j_l(k'r) \tag{32}$$

$$I^{(1)}_l(k, k') = \frac{\beta}{k'} \int dr\, r^2\, k\, \frac{d}{dr}\left(\phi(r) j_l(kr)\right)\, j'_l(k'r). \tag{33}$$

The lowest order corrections due to redshift space distortions are therefore encapsulated in $\Psi^{(1)}_{lm}(k)$. We can define a set of power spectra by using these harmonic coefficients:

$$\langle \Psi^{\alpha}_{lm}(k) \Psi^{\beta *}_{l'm'}(k') \rangle = \mathcal{C}^{(\alpha\beta)}_l(k, k') \delta_{1D}(k - k') \delta_{ll'} \delta_{mm'}, \tag{34}$$

$$\langle \Psi^{\alpha}_{lm}(k) \tilde{\Psi}^{\beta *}_{l'm'}(k') \rangle = \tilde{\mathcal{C}}^{(\alpha\beta)}_l(k, k') \delta_{ll'} \delta_{mm'}. \tag{35}$$

We can construct a generalised power spectrum by using the common structure between Eq.(30) and Eq.(31):

$$\tilde{\mathcal{C}}^{(\alpha\beta)}_l(k_1, k_2) = \left(\frac{2}{\pi}\right)^2 \int k'^2 dk' \; I^{(\alpha)}_l(k_1, k') I^{(\beta)}_l(k_2, k') P_{\delta\delta}(k'). \tag{36}$$

The total redshifted power spectrum will be given by a sum of the various contributions:

$$\tilde{\mathcal{C}}_l(k_1, k_2) = \tilde{\mathcal{C}}^{(00)}_l(k_1, k_2) + 2\, \tilde{\mathcal{C}}^{(01)}_l(k_1, k_2) + \tilde{\mathcal{C}}^{(11)}_l(k_1, k_2). \tag{37}$$

If we ignore the effects introduced by the selection function, i.e. set $\phi(r)$ = 1, then we recover the result of Castro, Heavens and Kitching (2005) for the unredshifted contributions:

$$\mathcal{C}^{(00)}_l(k, k) = P_{\delta\delta}(k). \tag{38}$$

These expressions hold for surveys with all-sky coverage. In the presence of homogeneity and isotropy the 3D power spectrum will be independent of radial wave number l. The introduction of a sky mask breaks isotropy and introduces additional mode-mode couplings, the analysis will be generalised to this case in the next section. In the above equations we neglect a number of additional non-linear terms including General Relativistic corrections, velocity terms and lensing terms. It is also possible to adopt a full non-linear approach to RSD where the non-linear spectrum has significantly more complicated angular structure than in linear theory Shaw and Lewis (2008). The RSD information will be dependent on the relative clustering amplitude of the transverse modes and the radial modes Asorey et al (2012). Our ability to recover information and the extent to which the information radialises will naturally depend on the geometry of the survey and which modes we are able to include.

2.5 Realistic Surveys

The results that have been discussed above are somewhat idealised in the sense that we assume all-sky coverage with no noise. In realistic surveys we will often need to take into account the presence of a mask (relating to partial sky-coverage) and noise. If the noise is inhomogeneous we will be presented with a further complication. For partial sky coverage we find mode-mode couplings in the harmonic domain that result in the individual masked harmonics being described by a linear combination of our idealised all-sky harmonics. We do not discuss the role of partial sky-coverage in much detail but do present results generalising our formalism to include a survey mask.

2.5.1 Partial-Sky Coverage and Mode Mixing

Large scale surveys do not, generally, have full-sky coverage. Instead the information regarding sky-coverage is encapsulated in a mask $\chi(\hat{\Omega})$ which is unity for areas covered in the survey and zero for regions outside the survey. The field harmonics are therefore modulated in the presence of a mask:

$$\tilde{\Psi}_{lm}(k) = \sqrt{\frac{2}{\pi}} \int s^2 ds \int d\hat{\Omega} \, \left[\phi(s)\chi(\hat{\Omega})\right] \Psi(\mathbf{r}) j_l(ks) Y^*_{lm}(\hat{\Omega}). \tag{39}$$

The convolved power-spectra in the presence of the mask takes the following form:

$$\tilde{\mathcal{C}}^{(\alpha\beta)}_l(k_1, k_2) = \left(\frac{2}{\pi}\right)^2 \sum_{l_a} \sum_{l_b} \int k' dk' \int k'' dk'' \times W^{(\alpha)}_{ll_a}(k_1, k') W^{(\beta)}_{ll_b}(k_2, k'') \frac{I_{ll_a l_b}}{(2l+1)} \mathcal{C}^{\chi}_{l_a} \mathcal{C}_{l_b}(k', k''); \tag{40}$$

$$\mathcal{C}^{\chi}_l = \langle \chi_{lm} \chi^*_{lm} \rangle \tag{41}$$

where $I_{l_1 l_2 l_3}$ is the Gaunt integral (see Eq.(B4)). The convolved power spectrum is a linear combination of all-sky spectra and depends on the power spectrum of the adopted mask (see Appendix-D for detailed derivations.).

2.5.2 Error Estimate

The signal to noise for individual modes for a given power-spectrum can be expressed as:

$$\frac{\delta \mathcal{C}_l(k, k)}{\mathcal{C}_l(k, k)} = \sqrt{\frac{2}{2l+1}} \left(1 + \frac{1}{\bar{n}\mathcal{C}_l(k, k)}\right) \tag{42}$$

Where $\bar{n}$ is the average number density of galaxies and the second term represents the leading order shot-noise contribution. For our results we take $\bar{n} = 10^{-3} h^3 \mathrm{Mpc}^{-3}$.

2.6 BAO Wiggles Only

The BAOs can be isolated by constructing a ratio between the observed matter power spectrum $P^{\rm B}_{\delta\delta}(k)$ and a theoretical matter power spectrum $P^{\rm nB}_{\delta\delta}(k)$ constructed from a zero-baryon transfer function in which the oscillations do not show up (Eisenstein et al 2005). Using these two power spectra, the ratio $R^P(k)$ will reduce the dynamic range and isolates the oscillatory features of the BAOs

$$R^P(k) = \frac{P^B(k)}{P^{nB}(k)}. \tag{43}$$

This ratio is clearly defined for the Fourier space power spectrum but an appropriate generalisation to the SFB formalism may be constructed by calculating the ratio of the angular power spectra defined in Equation (13), with the matter power spectrum $C_l^B(k)$ to the angular power spectrum with the zero-Baryon power spectrum $C_l^{nB}(k)$ (Rassat and Refregier 2012):

$$R_l^C(k) = \frac{C_l^B(k)}{C_l^{nB}(k)}. \tag{44}$$

It is important to note that the characterisation method (i.e. how we choose to construct our ratio) can affect the characteristic scale of the BAOs when we take into account non-linear effects. This means that care has to be taken when comparing results that implement different methods (Rassat et al 2008). As an example we could construct our ratio by using the No-Wiggles transfer function of Eisenstein et al (2005) or adopt an interpolation scheme to construct a smooth parametric curve Blake et al (2006); Percival et al (2007); Seo and Eisenstein (2007). A different choice of smoothed matter power spectra, cosmological parameters, growth history or similar can impact the phenomenological behaviour of the underlying physics (e.g. location of BAO peaks). Other methods for characterising the acoustic oscillation scales can be found, for example, in (Percival et al 2007; Nishimichi et al 2007).

3 NON-LINEAR CORRECTIONS

The role of nonlinear gravitational clustering can investigated in the spherical Fourier-Bessel formalism by incorporating higher order corrections to the power spectrum as described in perturbation theory. The approach we adopt here is standard perturbation theory (SPT) which provides a rigorous framework from which we can investigate the dependency of the radialisation of information on different parameters in a fully analytic manner (Vishniac 1983; Fry 1984; Goroff, Grinstein, Rey and Wise 1986; Suto and Sasaki 1991; Makino, Sasaki and Suto 1992; Jain and Bertschinger 1994; Scoccimarro and Frieman 1996). Standard perturbation theory is one of the most straightforward approaches to studies beyond linear theory and is based on a series solution to the hydrodynamical fluid equations in powers of an initial density or velocity field. The nonlinear clustering of matter arises from mode-mode couplings of density fluctuations and velocity

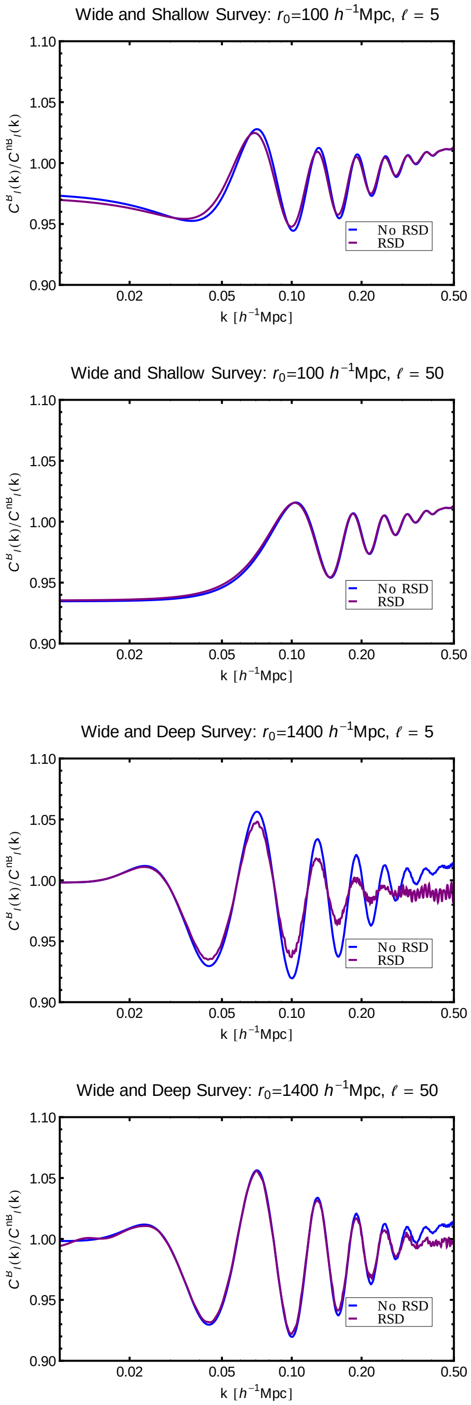

Figure 1. Slice in l-space showing $R_l^C(k)$ for $\ell = 5$ (top-panels) and $\ell = 50$ (bottom-panels) in a wide and shallow survey of $r_0 = 100h^{-1}$Mpc (left-panels) as well as for a deep survey of $r_0 = 1400h^{-1}$Mpc (right-panels). The solid-lines denote the $\mathcal{C}^{(00)}$ term and the dashed-lines show the total power-spectra.

divergence as seen from the Fourier space equations. The role of perturbation theory in the nonlinear evolution of the BAO in the power spectrum has been previously investigated (for an incomplete selection of references please see: Jeong and Komatsu (2006); Nishimichi et al (2007); Nomura, Yamamoto and Nishimichi (2008); Nomura, Yamamoto, Huetsi and Nishimichi (2009); Taruya, Nishimichi, Saito and Hiramatsu (2009); Taruya, Nishimichi and Saito (2010)). In this paper we generalise these investigations to the SFB approach.

Consider the hydrodynamic equations of motion for density perturbations δ such that our coming coordinates are denoted by $\mathbf{x}$ and the conformal time by η:

$$\delta'(\mathbf{x},\eta) + \nabla\cdot[(1+\delta(\mathbf{x},\eta))\mathbf{v}(\mathbf{x},\eta)] = 0, \tag{45}$$

$$\mathbf{v}'(\mathbf{x},\eta) + [\mathbf{v}(\mathbf{x},\eta)\cdot\nabla]\,\mathbf{v}(\mathbf{x},\eta) + \mathcal{H}(\eta)\mathbf{v}(\mathbf{x},\eta) = -\nabla\phi(\mathbf{x},\eta), \tag{46}$$

$$\nabla^2\phi(\mathbf{x},\eta) = \frac{3}{2}\mathcal{H}^2(\eta)\delta(\mathbf{x},\eta), \tag{47}$$

where a prime denotes the derivative with respect to the conformal time and $\mathcal{H} = a'/a$. The rotational mode of the peculiar velocity $\mathbf{v}$ is a decaying solution in an expanding universe and can be neglected in this approach. We introduce a scalar field describing the velocity divergence:

$$\Theta(\mathbf{x},\eta) = \nabla\cdot\mathbf{v}(\mathbf{x},\eta). \tag{48}$$

In our discussion we will focus on a description of the density perturbations and Fourier decompose the above equations to set up and solve a system of integro-differential equations. The Fourier decomposition of the perturbations are defined by:

$$\delta(\mathbf{x},\eta) = \int \frac{d^3k}{(2\pi)^3}\delta(\mathbf{k},\eta)e^{-i\mathbf{k}\cdot\mathbf{x}}, \tag{49}$$

$$\Theta(\mathbf{x},\eta) = \int \frac{d^3k}{(2\pi)^3}\Theta(\mathbf{k},\eta)e^{-i\mathbf{k}\cdot\mathbf{x}} \tag{50}$$

The equations of motion can be decomposed as follows:

$$\delta'(\mathbf{x},\eta) + \Theta(\mathbf{k},\eta) = -\int d^3k_1\int d^3k_2\delta^{(3)}(\mathbf{k}_1+\mathbf{k}_2-\mathbf{k}) \tag{51}$$
$$\frac{\mathbf{k}\cdot\mathbf{k}_1}{k_1^2}\Theta(\mathbf{k}_1,\eta)\delta(\mathbf{k}_2,\eta),$$

$$\Theta'(\mathbf{k},\eta) + \mathcal{H}(\eta)\Theta(\mathbf{k},\eta) + \frac{3}{2}\mathcal{H}^2(\eta)\delta(\mathbf{k},\eta) = \tag{52}$$
$$-\int d^3k_1\int d^3k_2\delta^{(3)}(\mathbf{k}_1+\mathbf{k}_2-\mathbf{k})\frac{k^2(\mathbf{k}_1\cdot\mathbf{k}_2)}{2k_1^2k_2^2}\Theta(\mathbf{k}_1,\eta)\Theta(\mathbf{k}_2,\eta).$$

In order to solve these coupled integro-differential equations we introduce a perturbative expansion of our variables

$$\delta(\mathbf{k},\eta) = \sum_{n=1}^{\infty} a^n(\eta)\delta_n(\mathbf{k}), \tag{53}$$

$$\Theta(\mathbf{k},\eta) = \mathcal{H}(\eta)\sum_{n=1}^{\infty} a^n(\eta)\Theta_n(\mathbf{k}). \tag{54}$$

The general n-th order solutions are given by:

$$\delta_n(\mathbf{k}) = \int d^3q_1\ldots\int d^3q_n\delta^{(3)}\left(\sum_{i=1}^{n}\mathbf{q}_i - \mathbf{k}\right)$$
$$\times F_n(\mathbf{q}_1,\ldots,\mathbf{q}_n)\Pi_{i=1}^{n}\delta_1(\mathbf{q}_i), \tag{55}$$

$$\Theta_n(\mathbf{k}) = -\int d^3q_1\ldots\int d^3q_n\delta^{(3)}\left(\sum_{i=1}^{n}\mathbf{q}_i - \mathbf{k}\right)$$
$$\times G_n(\mathbf{q}_1,\ldots,\mathbf{q}_n)\Pi_{i=1}^{n}\delta_1(\mathbf{q}_i), \tag{56}$$

where the kernels $F_n(\mathbf{q}_1,\ldots,\mathbf{q}_n)$ and $G_n(\mathbf{q}_1,\ldots,\mathbf{q}_n)$ are given by Jain and Bertschinger (1994)

$$F_n(\mathbf{q}_1,\ldots,\mathbf{q}_n) = \sum_{m=1}^{n-1}\frac{G_m(\mathbf{q}_1,\ldots,\mathbf{q}_m)}{(2n+3)(n-1)}$$
$$\times\left[(1+2n)\frac{\mathbf{k}\cdot\mathbf{k}_1}{k_1^2}F_{n-m}(\mathbf{q}_{m+1},\ldots,\mathbf{q}_n)\right.$$
$$\left.+\frac{k^2(\mathbf{k}_1\cdot\mathbf{k}_2)}{k_1^2k_2^2}G_{n-m}(\mathbf{q}_{m+1},\ldots,\mathbf{q}_n)\right], \tag{57}$$

$$G_n(\mathbf{q}_1,\ldots,\mathbf{q}_n) = \sum_{m=1}^{n-1}\frac{G_m(\mathbf{q}_1,\ldots,\mathbf{q}_m)}{(2n+3)(n-1)}$$
$$\times\left[3\frac{\mathbf{k}\cdot\mathbf{k}_1}{k_1^2}F_{n-m}(\mathbf{q}_{m+1},\ldots,\mathbf{q}_n)\right.$$
$$\left.+n\frac{k^2(\mathbf{k}_1\cdot\mathbf{k}_2)}{k_1^2k_2^2}G_{n-m}(\mathbf{q}_{m+1},\ldots,\mathbf{q}_n)\right], \tag{58}$$

The kernel $F_n(\mathbf{q}_1,\ldots,\mathbf{q}_n)$ is not symmetric under permutations of the argument $\mathbf{q}_1\ldots\mathbf{q}_n$ and must be symmetrised

$$F_n^{(s)} = \frac{1}{n!}\sum_{\text{Permutations}}F_n(\mathbf{q}_1,\ldots,\mathbf{q}_n). \tag{59}$$

As an example the second order symmetrised solution is given by

$$F_2^{(s)}(k_1,k_2) = \frac{5}{7} + \frac{2}{7}\frac{(\mathbf{k}_1\cdot\mathbf{k}_2)^2}{k_1^2k_2^2} + \frac{(\mathbf{k}_1\cdot\mathbf{k}_2)}{2}\left(\frac{1}{k_1^2}+\frac{1}{k_2^2}\right) \tag{60}$$

The corresponding second order matter power spectrum represents the linear matter power spectrum plus the additional higher order corrections. This calculation is made under the assumption that the first order density perturbations $\delta_1(\mathbf{k})$ constitute a Gaussian random field. The power spectrum up to second order is given by

$$P_{\rm SPT}(k,z) = D^2(z)P_{\rm lin}(k) + D^4(z)P_2(k), \tag{61}$$

where $P_{\rm lin}$ is the conventional linear matter power spectrum and the second order correction are given by

$$P_2(k) = P_{22}(k) + 2P_{13}(k). \tag{62}$$

These terms correspond to the contributions to the 4-point correlation function from the (2,2)-order and the (1,3)-order cross-correlations.

The explicit form of these terms is given by (for full equations see **??**)

$$P_{22}(k) = 2\int d^3q P_{\rm lin}(|\mathbf{k}-\mathbf{q}|)\left[F_2^s(\mathbf{q},\mathbf{k}-\mathbf{q})\right]^2, \quad (63)$$

$$P_{13}(k) = 3P_{\rm lin}(q)\int d^3q P_{\rm lin}(q)F_3^s(\mathbf{q},-\mathbf{q},\mathbf{k}). \quad (64)$$

It should be noted that the analytical predictions arising from standard perturbation theory will eventually break down as the non-linear terms become dominant over the linear theory predictions. Jeong and Komatsu (2006) demonstrated that one-loop standard perturbation theory was able to fit N-body simulations to greater than 1% accuracy when the maximum wave number $k_{1\%}$ satisfies (Taruya, Nishimichi, Saito and Hiramatsu 2009)

$$\frac{k_{1\%}^2}{6\pi^2}\int_0^{k_{1\%}} dq\ P_{\rm lin}(q;z) = C \quad (65)$$

where $C = 0.18$ in standard perturbation theory. SPT theory relies on a straightforward expansion of the set of cosmological hydrodynamical equations and the approach has been repeatedly noted as being insufficiently accurate to model and describe the BAOs (Jeong and Komatsu 2006; Taruya, Nishimichi, Saito and Hiramatsu 2009; Nishimichi et al 2009; Carlson, White and Padmanabhan 2009; Taruya, Nishimichi and Saito 2010). In particular the amplitude of SPT predicts a monotonically increase with the wavenumber overestimating the amplitude (Figure 2) with respect to N-body simulations Taruya, Nishimichi, Saito and Hiramatsu (2009).

Note that we have divided the nonlinear power spectrum by a smooth linear power spectrum when constructing the ratio $R_l^C(k)$ highlighting the scale dependence introduced by mode coupling. An alternative possibility would be to divide the nonlinear power spectrum $P^{\rm NL}$ by a nonlinearly evolved smooth power spectrum $P^{\rm NL}_{\rm smooth}$ removing this scale dependence and providing a more detailed comparison of PT predictions against numerical simulations. We leave such a comparison to future work.

Although we have not presented alternative approaches to PT there are a number of immediate extensions to this work that will be explored in upcoming papers. As future wide field surveys will cover both wide and deep regions of the sky we can use the SFB formalism as a tool to distinguish between different models for non-linear evolution of the matter density field. How do different theories affect the radial and tangential modes? How do different models affect the radialisation of information at various redshifts?

We will compare different approaches to cosmological perturbation theory and investigate the power of the SFB formalism as a tool for model testing in forthcoming work. The role of other additional non-linearities, such as non-Gaussianity and modified galaxy clustering bias models, will be presented in future work.

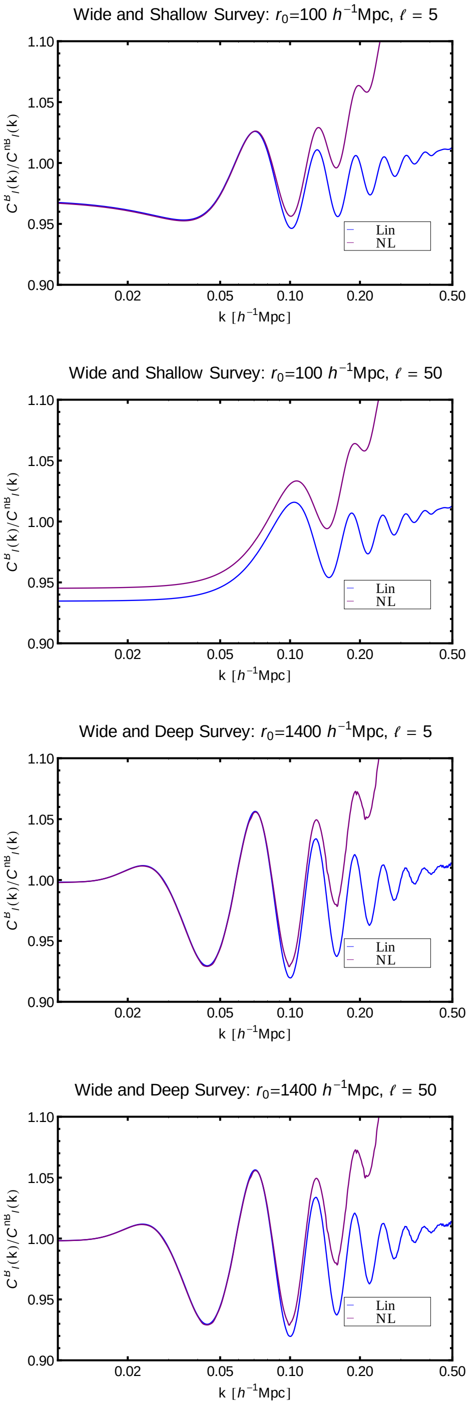

Figure 2. Slice in l-space showing $R_l^C(k)$ for $\ell = 5$ (top-panels) and $\ell = 50$ (bottom-panels) in a wide and shallow survey of $r_0 = 100h^{-1}$Mpc (left-panels) as well as for a deep survey of $r_0 = 1400h^{-1}$Mpc (right-panels). The solid-lines denote the results of linear calculations and the dashed-lines show the total power-spectra computed by taking one-loop corrections into account.

4 RESULTS

Following Rassat and Refregier (2012) we construct the quantity $R_l^C(k)$ to isolate the BAOs in the SFB formalism. The matter power spectrum, as defined in Eqn. (36) includes the physical effects of baryons leading to the characteristic oscillations as seen in Fourier space (Sunyaev and Zeldovich 1970; Peebles and Yu 1970; Seo and Eisenstein 2003, 2007).

In Figure [1] we construct slices of constant l through $R_l^C(k)$ to investigate how non-linearities manifest themselves in the oscillations. Rassat and Refregier (2012) used such slice plots to investigate the radialisation of information when varying levels of tangential and radial information is included in a survey. The radialisation of information can be investigated by notion that in the limit $r_0 \to \infty$ we find

$$\lim_{r_0 \to \infty} R_l^C(k) = R^P(k) = \frac{P^B(k)}{P^{nB}(k)}. \tag{66}$$

Radialisation means that $R_l^C(k)$ tends towards $R^P(k)$ in both phase and amplitude. This occurs as the tangential modes are attenuated due to mode-cancelling along the line of sight (Rassat and Refregier 2012). The radialisation can be seen in Figures [1] and [2] (linear and un-redshifted lines) where the amplitude of the first peak is higher in the wide and deep survey than in the wide and shallow survey. Additionally the BAOs appear to only have a radial (k) dependence in surveys with a large radial parameter r_0, as can be seen by the invariance the BAOs under a varying multipole l. The addition of redshift space distortions does not change this trend drastically though we do see more prominent radial and tangential dependence in Figure [1] with the rate at which the BAOs radialise being naturally impacted due to mode-mixing, attenuation and peak shifts. The results appear to be in agreement with previous studies with percent level shifts in the peaks to smaller k and damping of the amplitude (Nishimichi et al 2007; Nomura, Yamamoto and Nishimichi 2008; Smith, Scoccimarro and Sheth 2008; Nomura, Yamamoto, Huetsi and Nishimichi 2009; Taruya, Nishimichi and Saito 2010). As can be seen in Figure [1] the BAOs seem to radialise, even in the presence of RSD, at large values of the radius parameter r_0, notably so for large multipoles l as we would anticipate (Rassat and Refregier 2012).

The BAOs, as realised in SFB space, radialise as the survey size, r_0, is increased. This corresponds to the amplitude and the phase of the BAOs tending towards the values as measured in the Fourier space ratio $R^P(k)$. As noted in Rassat and Refregier (2012), for a wide-field shallow survey the BAO will have smaller amplitudes and are spread across the (l, k) space. However, in a wide-field deep survey the unredshifted BAOs have larger amplitudes and are confined to the radial modes (e.g. we have lost the tangential, l-mode dependence). It was shown in Rassat and Refregier (2012) that the BAOs appear to radialise before the full SFB spectrum is able to and notably so at large l (Figures [3-4]), one of the key motivations for implementing the SFB formalism.

As can be seen, when the RSD are included then the radialisation of information is damped and there is an increased dependence on the information contained in the tangential modes for genuine radialisation to occur. The non-linear corrections, in contrast, radialise as expected but there is an increased dependence on tangential modes in the shallow surveys with the amplitude of the BAOs being amplified when higher l-modes are taken into account.

5 CONCLUSION

The baryon acoustic oscillations give rise to a characteristic signature in the observed matter power spectrum that acts as a standard ruler. Unfortunately, the observed matter power spectrum is contaminated and complicated by non-linearities arising from the evolution of density perturbations, galaxy clustering bias, redshift space distortions and survey specific systematic errors. In addition, upcoming future surveys will cover both large and deep areas of the sky demanding a formalism that simultaneously treats the both the spherical sky geometry and the extended radial coverage. A spherical Fourier-Bessel basis was proposed as being a natural basis for random fields in this geometry. The recent study by Rassat and Refregier (2012) was an initial step into investigating the role of the SFB formalism in the study and analysis of the BAO. This study, however, did not go as far as including higher order contributions to the power spectrum that may impact the radialisation of information by introducing, for example, mode-mode couplings. The stability of this radialisation of information and the information content of tangential (l) and radial (k) modes for higher order physics is the key topic of interest.

In this paper we have presented a short treatment of the effects of redshift space distortions and non-linear corrections to measurements of baryon acoustic oscillations in the spherical Fourier-Bessel expansion. In order to guide this investigation we have extended the formalism and techniques outlined in Rassat and Refregier (2012). In particular we have been able to use the procedure outlined in Heavens and Taylor (1995) to construct a series expansion solution to model redshift space distortions. This solution was used to numerically and analytically investigate the modulation to the angular SFB power spectrum. The qualitative behaviour of these corrections was outlined for surveys with varying levels of radial (k-modes) and tangential (l-modes) information. It was seen that the RSD impact the radialisation of information through mode-mixing and the distinct signature was investigated over a range of survey configurations. The appropriate formalism for partial-sky coverage was also introduced and outlined for which results will be presented in forthcoming work.

The second main non-linearity investigated was one-loop corrections to the matter power spectrum arising from standard perturbation theory. A brief outline of perturbation theory methods was given and the basic equations for SPT introduced. The non-linear corrections and impact on radialisation of BAOs in the SFB was numerically investigated. Possible parallel studies may include the analysis of different perturbation theory methods and their ability to influence the radialisation of information as well as the possibility of distinguishing between theories for the non-linear corrections to the matter power spectrum and, consequentially, the BAO signal. Additionally we have neglected a detailed analysis of non-linear galaxy biasing models

In this paper we have neglected other contributions to the power spectrum such as General Relativistic corrections, lensing terms, the role of non-linearities through more detailed studies, more complex treatments of galaxy biasing and more detailed modelling of the

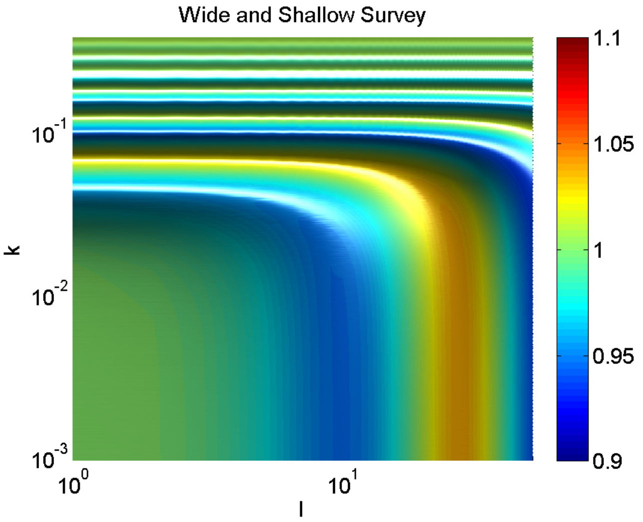

Figure 3. Ratio $R_l^C(k)$ of SFB spectrum with and without the physical effects of baryons in (l,k) phase space for a wide and shallow survey of $r_0 = 100h^{-1}$Mpc using a Gaussian selection function. The baryonic wiggles are seen in both the radial (k) and tangential (ℓ) directions.

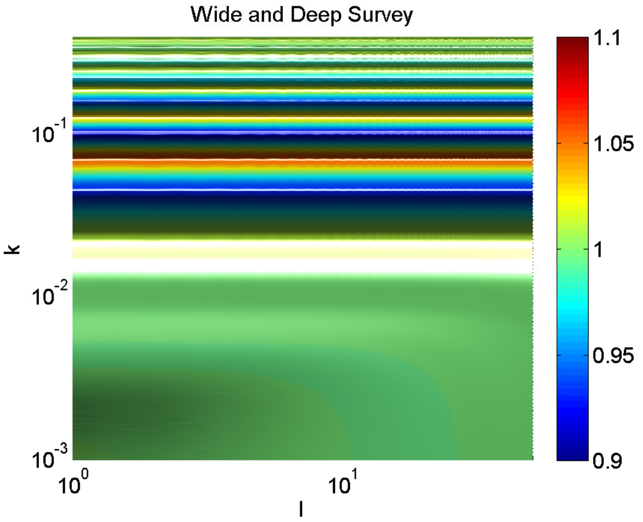

Figure 4. Ratio $R_l^C(k)$ of SFB spectrum with and without the physical effects of baryons in (ℓ,k) phase space for a wide and deep survey of $r_0 = 1400h^{-1}$Mpc using a Gaussian selection function. The baryonic wiggles are seen in both the radial (k) and tangential (ℓ) directions.

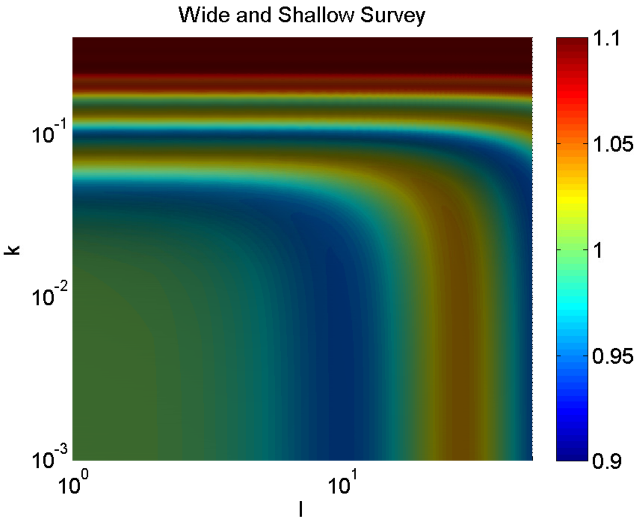

Figure 5. Ratio $R_l^C(k)$ of SFB spectrum with and without the physical effects of baryons in (l,k) phase space for a wide and shallow survey of $r_0 = 100h^{-1}$Mpc using a Gaussian selection function but with the inclusion of non-linear features as calculated in Standard Perturbation Theory.

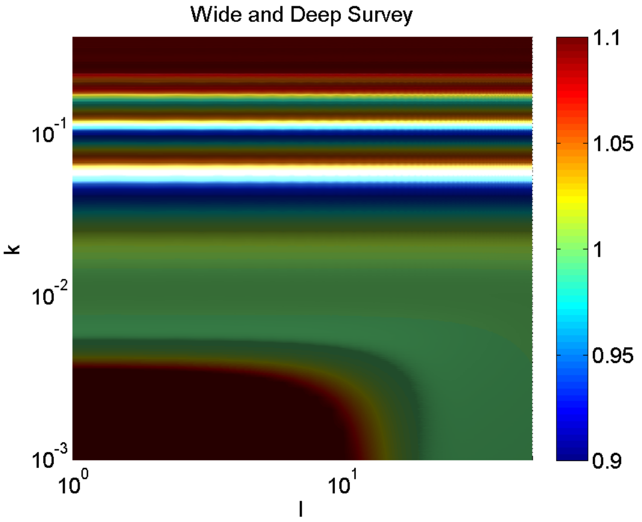

Figure 6. Ratio $R_l^C(k)$ of SFB spectrum with and without the physical effects of baryons in (ℓ,k) phase space for a wide and deep survey of $r_0 = 1400h^{-1}$Mpc using a Gaussian selection function but with the inclusion of non-linear features as calculated in Standard Perturbation Theory.

hydrodynamical and radiative processes involved in these processes (Guillet et al 2010; Juszkiewicz, Hellwing and van de Weygaert 2012). In addition we have not considered the role of systematic errors in a particular survey and how they may affect the radial and tangential measurements in different ways and consequentially complicate the analysis of BAOs. We leave this to a future paper but note that the results in Asorey et al (2012) will be of interest.

6 ACKNOWLEDGEMENTS

DM acknowledges support from STFC standard grant ST/G002231/1 at the School of Physics and Astronomy at Cardiff University where this work was completed. Its a pleasure to thanks Peter Coles and Alan Heavens, for many useful discussions.

REFERENCES

Abramo L. R., Reimberg P. H., Xavier H. S., 2010, PRD, 82, 043510, arXiv:1105.0563
Adelman-McCarthy J. K., Ageros M.A., Allam S.S., et al., 2008, ApJS, 175, 297
Alam U., Sahni V., 2006, PRD, 73, 084024, arXiv:astro-ph/0511473
Alcock C., Paczynski B., 1979, Nat., 281, 358
Amendola L., Quercellini C., Giallongo E., 2005, MNRAS, 357, 429, arXiv:astro-ph/0404599
Annis J., et al., The Dark Energy Task Force, 2005, arXiv:astro-ph/0510195
Asorey J., Crocce M., Gaztanaga E., Lewis A., 2012, arXiv:1207.6487
Banerji M., Abdalla F.B., Lahav O., Lin H., 2008, MNRAS, 386, 1219, arXiv:0711.1059v2
Bentez N., et al., 2009, APJ, 691, 241, arXiv:0807.0535v4
Binney J., Quinn T., 1991, MNRAS, 241, 678
Blake C., Parkinson D., Bassett B., Glazebrook K., Kunz M., Nichol R. C., 2006, MNRAS, 365, 255, arXiv:astro-ph/0510239
Carlson J., White M., Padmanabhan N., 2009, PRD, 80, 043531, arXiv:0905.0479
Castro P.G., Heavens A.F., Kitching T.D., 2005, PRD, 72, 023516, arXiv:astro-ph/0503479
Challinor A., Lewis A., 2011, PRD, 84, 043516, arXiv:1105.5292
Coles P., Erdogdu P., 2007, JCAP, 0710, 007, arXiv:0706.0412
Colless M., et al., 2003, arXiv:astro-ph/0306581, "The 2dF Galaxy Redshift Survey: Final Data Release"
Crocce M., Fosalba P., Castander F.J., Gaztanaga E., 2010, MNRAS, 403, 1353, arXiv:0907.0019
Dolney D., Jain B., Takada M., 2006, MNRAS, 366, 884-898, arXiv:astro-ph/0409445
Eisenstein D.J., Zehavi I., Hogg D.W., Scoccimarro R., et al., 2005, APJ, 633, 560, arXiv:astro-ph/0501171
Erdogdu P., et al., 2006, MNRAS, 373, 45-64, arXiv:astro-ph/0610005
February S., Clarkson C., Maartens R., 2012, arXiv:1206.1602
Fisher K.B., Lahav O., Hoffman Y., Lynden-Bell D., Zaroubi S., 1995, MNRAS, 272, 885, arXiv:astro-ph/9406009
Fry J. N., 1984, ApJ, 279, 499
Garcia-Bellido J., Haugboelle T., 2008, JCAP, 0804, 003, arXiv:0802.1523
Garcia-Bellido J., Haugboelle T., 2009, JCAP, 0909, 028, arXiv:0810.4939
Gaztanaga E., et al., 2011, arXiv:1109.4852
Goroff M., Grinstein B., Rey S.-J., Wise M., 1986, ApJ, 311, 6
Goobar A., Hannestad S., Mrtsell E., Tu H., 2006, JCAP, 6, 19, arXiv:astro-ph/0602155
Guillet T., Teyssier R., Colombi S., 2010, MNRAS, 405, 525, arXiv:0905.2615
Heavens A., Taylor A., 1995, MNRAS, 275, 483, arXiv:astro-ph/9409027
Hirata C., 2009, MNRAS, 399, 1074, arXiv:0903.4929
Hivon E., Grski K.M., Netterfield C.B., Brill B.P., Prunet S., Hansen F., 2002, APJ, 567, 2, arXiv:astro-ph/0105302
Huchra J.P., et al., 2011, arXiv:1108.0669
Jain B., Bertschinger E., 1994, ApJ, 431, 495-505, arXiv:astro-ph/9311070
Jeong D., Komatsu E., 2006, ApJ, 651, 619-626, arXiv:astro-ph/0604075
Jeong, D., Komatsu, E., 2009, ApJ, 691, 569, arXiv:0805.2632
Juszkiewicz R., Hellwing W.A., van de Weygaert R., 2012, arXiv:1205.6163v1
Komatsu E., et al., ApJS, 192, 18, arXiv:1001.4538
Lanusse F., Rassat A., Starck J.-L., 2012, A&A, 540, A92, arXiv:1112.0561
Laureijs R., et al., 2011, arXiv:1110.3193
Lazkoz R., Maartens R., Majerotto E., 2006, PRD, 74, 083510, arXiv:astro-ph/0605701
Leistedt B., Rassat A., Refregier A., Strack J.-L., 2011, arXiv:1111.3591
Makino N., Sasaki M., Suto Y., 1992, PRD, 68, 46, 585
Nishimichi T., et al., 2007, PASJ, 59, 1049, arXiv:0705.1589
Nishimichi T., et al., 2009, Publ. Astron. Soc. Jpn., 61, 321, arXiv:0810.0813
Nock K., Percival W.J., Ross A.J., 2010, MNRAS, 407, 520, arXiv:1003.0896
Nomura H., Yamamoto K., Nishimichi T., 2008, JCAP, 0810, 031, arXiv:0809.4538
Nomura H., Yamamoto K., Huetsi G., Nishimichi T., 2009, PRD, 79, 063512, arXiv:0903.1883
Padmanabhan N., et al., 2005, MNRAS, 359, 237, arXiv:astro-ph/0407594
Padmanabhan N., White M., Cohn J.D., 2009, PRD, 79, 063523, arXiv:0812.2905
Peebles P.J.E., Yu J.T., 1970, APJ, 162, 815
Percival W.J., Burkey D., Heavens A., et al., 2004, MNRAS, 353, 1201, arXiv:astro-ph/0406513
Percival W.J., Cole S., Eisenstein D.J., Nichol R.C., Peacock J.A., Pope A.C., Szalay A.S., 2007, MNRAS, 381, 1053, arXiv:0705.3323

Percival W. J., et al., 2007, ApJ, 657, 51, arXiv:astro-ph/0608635

Rassat A., et al., 2008, arXiv:0810.0003v1 [astro-ph]

Rassat A., Refregier A., 2012, arXiv:1112.3100

Ross A.J., Percival W.J., Crocce M., Cabr A., Gaztanaga E., 2011, MNRAS, 415, 3, 2193-2204, arXiv:1102.0968

Seo H.-J., Eisenstein D.J., 2003, ApJ, 598, 720, arXiv:astro-ph/0307460

Seo H.-J., Eisenstein D.J., 2007, ApJ, 665, 14, arXiv:astro-ph/0701079

Scoccimarro R., Frieman J., 1996, ApJ, 473, 620, astro-ph ¿ arXiv:astro-ph/9602070

Shapiro C., Crittenden R.G., Percival W.J., 2011, MNRAS, 422, 2341-2350, arXiv:1109.1981

Shaw J. R., Lewis A., 2008, PRD, 78, 103512, arXiv:0808.1724

Smith R.E., Scoccimarro R., Sheth R.K., 2008, PRD, 77, 043525, arXiv:astro-ph/0703620

Slosar A., Ho S., White M., Louis T., 2009, JCAP, 10, 19, arXiv:0906.2414

Sunyaev R.A., Zeldovich Y.B., 1970, apss, 7, 3

Suto Y., Sasaki M., 1991, PRL, 66, 264

Taruya A., Nishimichi T., Saito S., Hiramatsu T., 2009, PRD, 80, 123503, arXiv:0906.0507

Taruya A., Nishimichi T., Saito S., 2010, PRD, 82, 063522, arXiv:1006.0699

Umeh O., Clarkson C., Maartens R., 2012, arXiv:1207.2109, arXiv:1207.2109

Vishniac E., 1983, MNRAS, 203, 345

Wang Y., Mukhurjee P., 2006, APJ, 650, 1, arXiv:astro-ph/0604051

Xu X., et al., 2010, ApJ, 718, 1224, arXiv:1001.2324

York D.G., et al., 2000, AJ, 120, 1579, arXiv:astro-ph/0006396

APPENDIX A: SPHERICAL BESSEL FUNCTION

$$\int_0^\infty r^2 dr\, j_l(kr) j_l(k'r) = \frac{\pi}{2kk'}\delta(k-k') \tag{A1}$$

The first derivative of the spherical Bessel function can be expressed using the following recursion relation:

$$j_l'(r) = \frac{1}{2l+1}\Big[l j_{l-1}(r) - (l+1) j_{l+1}(r)\Big]. \tag{A2}$$

The second- and higher-order derivatives are deduced by successive application of the above expression:

$$\begin{aligned} j_l''(r) = \Big[&\frac{(2l^2+2l-1)}{(2l+3)(2l+1)} j_l(r) - \\ &- \frac{l(l-1)}{(2l-1)(2l+1)} j_{l-2}(r) - \frac{(l+1)(l+2)}{(2l+1)(2l+3)} j_{l+2}(r)\Big]. \end{aligned} \tag{A3}$$

These expressions can be used to simply the kernels $I_l^{(1)}(k,k')$ defined in Eqn.(33) to express mode-mixing due to redshift-space distortion.

APPENDIX B: SPHERICAL HARMONICS

The spherical-harmonics are complete and orthogonal on the surface of the sphere:

$$\sum_{lm} Y_{lm}(\hat\Omega) Y_{lm}(\hat\Omega') = \delta^{\rm 2D}(\hat\Omega - \hat\Omega') \tag{B1}$$

$$\int d\hat\Omega\; Y_{lm}(\hat\Omega) Y_{l'm'}(\hat\Omega') = \delta^{\rm K}_{ll'}\delta^{\rm K}_{mm'}. \tag{B2}$$

The overlap integrals of three spherical harmonics are given by the Gaunt integral which are expressed in terms of 3j symbols (denoted by matrices below):

$$\begin{aligned} \int d\hat\Omega Y_{lm}(\hat\Omega) Y_{l'm'}(\hat\Omega) Y_{l''m''}(\hat\Omega) &= I_{l_1 l_2 l_3} \\ \times \begin{pmatrix} l_1 & l_2 & l_3 \\ 0 & 0 & 0 \end{pmatrix} &\begin{pmatrix} l_1 & l_2 & l_3 \\ m_1 & m_2 & m_3 \end{pmatrix} \end{aligned} \tag{B3}$$

$$I_{l_1 l_2 l_3} = \sqrt{\frac{(2l_1+1)(2l_2+1)(2l_3+1)}{4\pi}}. \tag{B4}$$

APPENDIX C: 3J SYMBOLS

The following orthogonality properties of $3j$ symbols were used to simplify various expressions.

$$\begin{aligned} \sum_{l_3 m_3} (2l_3+1) \begin{pmatrix} l_1 & l_2 & l_3 \\ m_1 & m_2 & m_3 \end{pmatrix} \begin{pmatrix} l_1 & l_2 & l \\ m_1' & m_2' & m \end{pmatrix} \\ = \delta^{\rm K}_{m_1 m_1'} \delta^{\rm K}_{m_2 m_2'}; \end{aligned} \tag{C1}$$

$$\begin{aligned} \sum_{m_1 m_2} \begin{pmatrix} l_1 & l_2 & l_3 \\ m_1 & m_2 & m_3 \end{pmatrix} \begin{pmatrix} l_1 & l_2 & l_3' \\ m_1 & m_2 & m_3' \end{pmatrix} \\ = \frac{\delta^{\rm K}_{l_3 l_3'} \delta^{\rm K}_{m_3 m_3'}}{2l_3+1}; \end{aligned} \tag{C2}$$

APPENDIX D: FINITE SURVEYS AND DISCRETE SPHERICAL BESSEL-FOURIER TRANSFORMATION AND PSEUDO-$\mathcal{C}_L$S

D1 3D Scalar fields

Different types of boundary conditions are employed in the literature for finite surveys (Binney and Quinn 1991; Fisher et al 1995; Heavens and Taylor 1995).

A natural choice for the boundary condition is to assume that the field vanishes at the boundary of the survey $r = R$ leading to following condition on the radial modes that is determined by the zeros of the spherical Bessel functions $j_l(r)$:

$$j_l(q_{ln}) = j_l(k_{ln}R) = 0; \qquad q_{ln} = k_{ln}R. \tag{D1}$$

The closure relation for spherical harmonics will take the following form:

$$\int_0^1 dz\; z^2 j_l(k_{nl}z) j_l(k_{nl}z) = \frac{1}{2}[j_{l+1}(q_{ln})]^2 \delta_{ll'}\delta_{nn'}. \qquad \text{(D2)}$$

Which, in terms of the radial wavenumber, can be expressed as follows:

$$\int_0^R dr\; r^2 k_{ln} k_{l'n'} j_l(k_{ln}r) j_{l'}(k_{l'n'}r) = \frac{k_{ln}^2 [j_{l+1}(q_{ln})]^2}{2R^{-3}} \delta_{ll'}\delta_{nn'}. \qquad \text{(D3)}$$

The discrete spectrum is determined by the zeros of the spherical Bessel function. The normalisation coefficients are given by:

$$\frac{1}{\tau_{ln}} = \frac{R^3}{2}[k_{ln} j_{l+1}(k_{ln}R)]^2. \qquad \text{(D4)}$$

The inverse and forward discrete SFB transforms are as follows:

$$\Psi_{lm}(k_{ln}) = \tau_{ln} \int d^3\mathbf{r}\; \Psi(\mathbf{r}) j_l(kr) Y_{lm}(\hat{\Omega}); \qquad \text{(D5)}$$

$$\Psi(\mathbf{r}) = \sum_{lmn} \tau_{ln} \Psi_{lm}(k) j_l(kr) Y_{lm}(\hat{\Omega}). \qquad \text{(D6)}$$

The following expression is useful:

$$\Psi_{lm}(k_{ln}) = \frac{i^l}{(2\pi)^{3/2}} \int d\hat{\Omega}_k \Psi(k_{ln}, \hat{\Omega}_k) Y_{lm}(\hat{\Omega}_k) \qquad \text{(D7)}$$

In case of finite survey the 3D power-spectrum samples only discrete radial wave-numbers k_{ln} which is defined by the survey radius R:

$$\langle \Psi_{lm}(k_{ln}) \Psi^*_{l'm'}(k_{l'n'}) \rangle = P_{\Psi\Psi}(k_{ln}) \delta_{ll'}\delta_{mm'}\delta_{nn'} \qquad \text{(D8)}$$

In addition to finite survey size, surveys often have a mask $s(\hat{\Omega})$. The SFB transform of a masked field defines the convolved or *Pseudo* harmonics $\tilde{\Psi}_{lm}(k_{ln})$:

$$\begin{aligned} \tilde{\Psi}_{lm}(k_{ln}) = \quad & \sqrt{\frac{2}{\pi}} \tau_{ln} \int_0^R r^2 dr \int_\Omega d\hat{\Omega} \\ & \times [\phi(r) s(\hat{\Omega})] \Psi(\mathbf{r}) j_l(k_{ln}r) Y_{lm}(\hat{\Omega}) d\hat{\Omega} \end{aligned} \qquad \text{(D9)}$$

The convolved or *Pseudo*-harmonics are expressed in terms of all-sky harmonics $\Psi_{lm}(k_{ln})$ by the following expression:

$$\begin{aligned} \tilde{\Psi}_{lm}(k_{ln}) = \quad & \sum_{n'} \sum_{l'm'} \sum_{l''m''} \tau_{l'n'} W(k_{ln}, k_{l'n'}) \Psi_{lm}(k_{l'n'}) \\ & \times s_{l''m''} I_{ll'l''} \begin{pmatrix} l & l' & l'' \\ m & m' & m'' \end{pmatrix} \end{aligned} \qquad \text{(D10)}$$

The kernel $W(k_{ln}, k_{l'n'})$ depends on selection function $\phi(r)$:

$$W(k_{ln}, k_{l'n'}) = \int_0^R r^2\; dr\; \phi(r) j_l(k_{ln}r) j_l(k'_{l'n'}r) \qquad \text{(D11)}$$

The Pseudo-$\mathcal{C}_l$s (PCLs) constructed from the convolved harmonics are a function of power spectrum of the angular mask $\mathcal{C}^{\chi}_{l''}$, normalisation coefficients τ_{ln} and the selection function ϕ.

$$\begin{aligned} \tilde{\mathcal{C}}_l(k_{ln}) \quad & = \langle \tilde{\Psi}_{lm}(k_{ln}) \tilde{\Psi}^*_{lm}(k_{ln}) \rangle \\ & = \sum_{n'} \sum_{l'} \sum_{l''} \tau^2_{l'n'} \frac{I^2_{ll'l''}}{2l+1} \begin{pmatrix} l & l' & l'' \\ 0 & 0 & 0 \end{pmatrix}^2 \\ & \times W^2(k_{ln}, k_{l'n'}) \mathcal{C}_{l'}(k_{l'n'}) \mathcal{C}^{\chi}_{l''} \end{aligned} \qquad \text{(D12)}$$

Notice that the PCls $\tilde{\mathcal{C}}_l(k_{ln})$ are linear superposition of the power spectrum of underlying field $\mathcal{C}_l(k_{ln})$. The mixing matrix $M_{ln,l'n'}$ is given by:

$$\tilde{\mathcal{C}}_l(k_{ln}) = \sum_{l'n'} M_{ln,l'n'} \mathcal{C}_l(k_{l'n'}); \qquad \text{(D13)}$$

where the mixing matrix is given by the following expression:

$$M_{ln,l'n'} = \sum_{l''} \tau^2_{l'n'} \frac{I^2_{ll'l''}}{2l+1} \begin{pmatrix} l & l' & l'' \\ 0 & 0 & 0 \end{pmatrix}^2 W^2(k_{ln}, k_{l'n'}) \mathcal{C}^{\chi}_{l''}. \qquad \text{(D14)}$$

An unbiased estimates of the 3D power spectra can be written as:

$$\mathcal{C}_l(k_{ln}) = \sum_{l'n'} M^{-1}_{ln,l'n'} \tilde{\mathcal{C}}_l(k_{l'n'}). \qquad \text{(D15)}$$

This is an extension of well known results for the projected surveys (Hivon, Grski, Netterfield, Brill, Prunet and Hansen 2002). For low sky-coverage and small survey volumes the matrix $M_{ln,l'n'}$ is expected to be singular and binning of modes may be required.

A different choice of boundary condition is often employed (Fisher et al 1995):

$$j_{l-1}(k'_{ln}R) = 0; \qquad \text{(D16)}$$

The normalisation constants in this case are given by:

$$\frac{1}{\tau_{ln}} = \frac{R^3}{2}[k_{ln} j_l(k_{ln}R)]^2. \qquad \text{(D17)}$$

The expressions for the mixing matrix derived above can still be used simply replacing the normalisation coefficients τ_{ln}.

For discrete fields such as the galaxy distribution we can use the PCL approach if we replace the continuous function $\Psi(\mathbf{r})$ with a sum of delta functions that peak at galaxy positions r_s: $\Psi(\mathbf{r}) = \sum_{s=1}^{\mathrm{N}} \delta^{\mathrm{3D}}(\mathbf{r} - \mathbf{r}_s)$; here N is the number of galaxies. The SFB for such a discrete field is given by $\Psi_{lm}(k) = \sum_{s=1}^{N} \tau_{lm} j_l(r_s k_{ln}) Y_{lm}(\hat{\Omega}_s)$. Where the radial and angular position of galaxies are denoted by $\mathbf{r}_s = (r_s, \hat{\Omega}_s) = (r_s, \theta_s, \phi_s)$

APPENDIX E: STANDARD PERTURBATION THEORY

In the formalism outlined in section 3, any statistical observable can be computed to arbitrary order. Typically we are only interested in the second order corrections to the matter power spectrum though expressions for higher-order corrections have been derived. One of the key issues regarding the inclusion is the computational costs required for these higher order corrections in part due to the high dimensionality of the integrals, even after symmetry arguments have been taken into account. The analytic expressions for the first corrections can be analytically derived Makino, Sasaki and Suto (1992)

$$P_{13}(k) = \frac{1}{252}\frac{k^3}{4\pi^2}\int_0^\infty dx P_{\rm lin}(k) P_{\rm lin}(kx)\Bigg[\frac{12}{x^2} - 158 + 100x^2 \tag{E1}$$

$$- 42x^4 + \frac{3}{x^2}\left(x^2-1\right)^3\left(7x^2+2\right)\log\left|\frac{1+x}{1-x}\right|\Bigg]$$

$$P_{22}(k) = \frac{1}{98}\frac{k^3}{4\pi^2}\int_0^\infty dx P_{\rm lin}(kx)\int_{-1}^{1} d\mu P_{\rm lin}(k\sqrt{1+x^2-2x\mu}) \tag{E2}$$

$$\times \frac{\left(3x+7\mu-10x\mu^2\right)^2}{\left(1+x^2-2x\mu\right)^2}.$$